PHYSICAL REVIEW C **84**, 065205 (2011)

Nuclear attenuation at low energies

L. Grigoryan*
Yerevan Physics Institute, Brothers Alikhanian 2, 375036 Yerevan, Armenia
(Received 16 April 2011; revised manuscript received 22 October 2011; published 22 December 2011)

Nuclear attenuation of the single hadron at low energies of the virtual photon ν ($\nu < 5$ GeV) is considered in the framework of the improved two-scale model, which is one of the versions of the string model. The model is used for a description of the ratio of the multiplicities of pions electroproduced on nuclear and deuterium targets as a function of the energy of virtual photons and the fractional energy of the pions. The final state interactions, which are essential in this energy range, are taken into account. A comparison with two sets of the experimental data obtained at JLab is performed. A satisfactory agreement of the theoretical calculations with the first set of data for the ratio of the multiplicities of positively charged pions on carbon, iron, and lead targets to that on the deuterium one is obtained. However, agreement with the second set of data for the ratio of the multiplicities of positively and negatively charged pions on the aluminum target to those on the deuterium one is poor. Possible reasons for this situation are discussed.

DOI: 10.1103/PhysRevC.84.065205 PACS number(s): 13.87.Fh, 13.60.Le, 21.65.−f

I. INTRODUCTION

The space-time evolution of the hadronization process, despite its importance, has received relatively little study. The study of the early stages of the hadronization process can shed additional light on the further evolution of the process. Semi-inclusive reactions on nuclear targets give the possibility to study the development of the hadronization process on the distances of a few Fermi, starting from the deep inelastic scattering (DIS) point. The nuclei behave as small bubble chambers in these reactions.

The nuclear attenuation (NA) of the high-energy hadrons is a well-known tool for the investigation of the early stages of the hadronization process.[1] Experimental and theoretical studies in this direction have been performed over the past three decades.

Experimental investigations were carried out at several accelerator centers in the wide region of the energies of virtual photons, for sets of different nuclear targets and different species of hadrons observed in the final state [1–6]. The studies revealed that in the range of "very high energies" of the virtual photons ($\nu > 50$ GeV for the NA) nuclear effects become irrelevant [2,3]. A possible explanation for this is that, due to the Lorentz boost formation, the lengths of the hadrons exceed the nuclear sizes at these energies and as a result the hadronization is realized beyond the nucleus. The range of "high energies" ($5 < \nu < 50$ GeV) is the most convenient for the study of NA since, at these energies, one side of the nuclear effects is large and from the other side the cascading effects are small. The experimental data in this energy range were obtained by the HERMES Collaboration [4–6]. The range of "low energies" ($\nu < 5$ GeV) has received very little study so far.

Over the past few decades many phenomenological models were developed that were able to describe NA [7–21]. Despite the variety of detail, these models can be divided into two groups in accordance with the mechanism lying at their base. At present, two basic mechanisms of NA are considered. (i) Hadronization occurs at distances comparable to the size of a nucleus, so NA is due to the absorption of the prehadrons and hadrons in nuclear matter [7–12,14,16–21]. (ii) The hadronization takes place at distances much larger than the size of a nucleus. The quark propagating in nuclear matter loses energy by gluon radiation, and thus the cause of NA is energy loss by a quark, which leads to the redefinition of the variables of the fragmentation function [13,15]. The string model that is considered in this paper is based on the first mechanism. A comparison with the experimental data must be the main method for the selection of more viable models. Unfortunately, the available data do not allow to make this selection. Additional data are needed.

At present, such data can be obtained at DESY and JLab. Recently, JLab presented two sets of data for NA [22–24]. These data belong to the range of "low energies" ($\nu < 5$ GeV). It is known that at these energies additional mechanisms can arise that make the theoretical study more complicated, in comparison with the "high energy" ($5 < \nu < 50$ GeV) case. We will try to describe the "low energy" data in the framework of the string model. It will be shown that calculations without invoking additional mechanisms (final state interactions or cascading process) underestimate the experimental data. The inclusion of the final state interactions (FSI) in the calculations allows to improve the agreement with the data. The main goal of this paper is the comparison of the string model with the JLab data at low energies and the estimation of the contribution of possible additional mechanisms. In these calculations we use the functions and parameters obtained as a result of a fit to the data of the HERMES experiment at DESY [20].

This paper is organized as follows. In Sec. II the theoretical model is briefly described. Results and discussion as well as the

*leva@mail.desy.de

[1]NA is the difference of the ratio of the multiplicities (per nucleon) on the nucleus to those on deuterium R_M^h from unity (i.e., $1 - R_M^h$).

necessary ingredients for calculations are presented in Sec. III. Our conclusions are given in Sec. IV.

II. THEORETICAL MODEL

We will consider the leptoproduction process of a single hadron in semi-inclusive deep inelastic scattering (SIDIS) on a nuclear target

$$l_i + A \to l_f + h + X, \tag{1}$$

where $l_i(l_f)$ is the initial (final) lepton and h is the observed hadron. The hadron h carries away a fraction z of the total available energy (in a fixed target system $z = E_h/\nu$, where E_h is the energy of the final hadron). The multiplicity ratio for that process, after averaging over the transverse momentum of the final hadron, has the form

$$R_M^h = \frac{2dN_A(\nu, Q^2, z)/dz}{AdN_D(\nu, Q^2, z)/dz}, \tag{2}$$

where dN_A/dz and dN_D/dz are the numbers of hadrons, carrying the fraction z of the total energy in the reaction (1) on the nuclear and deuterium targets, respectively, and $Q^2 = -q^2$, where q^2 is the square of the four-momentum of the virtual photon.

If we do not take into account the secondary interactions, dN_A/dz can be approximated by[2]

$$\frac{dN_A}{dz} \approx \frac{dN_A^{(0)}}{dz} = 2\pi A \int_0^\infty bdb \int_{-\infty}^\infty dx\rho(b,x) \times \int_x^\infty dx' D_c(L,z,x'-x) W_0(x,x'), \tag{3}$$

where b is the impact parameter, x is the longitudinal coordinate of the DIS point, $\rho(b,x)$ is the nuclear density function, x' is the longitudinal coordinate of the string-nucleon interaction point, and $D_c(L,z,l_c)$ is the distribution of the constituent formation length l_c of the hadrons carrying the energy fraction z [10,18] (L is the full hadronization length, $L = \nu/\kappa$, where κ is the string tension);

$$D_c(L,z,l) = L(1+C)\frac{l^C}{(l+zL)^{C+1}} \times \left(\delta(l-L+zL) + \frac{1+C}{l+zL}\right) \times \theta(l)\theta(L-zL-l), \tag{4}$$

where $C = 0.3$ is the parameter that controls the steepness of the fragmentation function in the standard Lund model. $W_0(x,x')$ is the probability that the leading quark, the first constituent of the observed hadron, and the observed hadron itself do not interact in the nuclear matter. A is the atomic mass number.

To make the model more realistic at low energies, we have to account for the yield of the secondary particles originating from the interactions produced in the DIS primary hadrons with intranuclear nucleons

$$\frac{dN_A^{(hi)}}{dz} = 2\pi \frac{A(A-1)}{2!} \int_0^\infty bdb \int_{-\infty}^\infty dx\rho(b,x) \int_z^1 \frac{dz'}{z'} \times \int_x^{x+L-z'L} dx' D_c(L,z',x'-x) W_{(hi)}(x,x'), \tag{5}$$

where z' is the fraction of the total available energy that carries the primary hadron, $W_{(hi)}(x,x')$ is the probability that the leading quark and the first constituent of the final hadron do not interact in the nuclear matter (the final hadron itself interacts in the nuclear matter inelastically only once). The above-presented probabilities have the form

$$W_0(x,x') = \left[1 - \int_x^\infty dx'' \sigma^{str}(\Delta x, l_c)\rho(b,x'')\right]^{A-1}, \tag{6}$$

where $\Delta x = x'' - x$, $l_c = x' - x$ and

$$W_{(hi)}(x,x') = \int_{x'+z'L}^\infty dx'' \Sigma d\sigma/d(z/z')\rho(b,x'') \times \left[1 - \int_x^\infty dx'' \sigma^{str}(\Delta x, l_c)\rho(b,x'')\right]^{A-2}, \tag{7}$$

where z/z' is the fraction of the energy of the primary hadron that carries away the final pion, $\Sigma d\sigma/d(z/z')$ is the sum of the inclusive cross sections for the hadron-nucleon interactions in the final state, leading to the production of the final pions, which are observed in the experiment.

Adding a term, which is responsible for the FSI, we can now write the expression for the number of hadrons, carrying away the fraction z of the total energy in the reaction (1) on the nuclear target

$$\frac{dN_A}{dz} = \frac{dN_A^{(0)}}{dz} + \frac{dN_A^{(hi)}}{dz}. \tag{8}$$

The string model is based on the idea that after DIS the knocked out (anti)quark does not leave the nucleon remnant, but forms a string (color dipole) with the (anti)quark on the fast ends and the nucleon remnant on the slow ends, while the color string itself consists of gluons. Its longitudinal size must be larger than the transverse one, but cannot be essentially larger than the hadronic size because of confinement. The string can break down into two strings according to the following scenarios. First, when the quark-antiquark pair from the color field of the string is produced and second, when the color interaction between the string and the nucleon (lying on its trajectory) has occurred (see, for instance, Refs. [8,19]). In the "history" of the string there are two time scales that are of interest to us. They are the time scales connected with the production of the first constituent (anti)quark of the final hadron and the interaction of its two constituents for the first time. These two scales are as follows: τ_c (l_c) is the constituent formation time (length)[3]

[2] In this section we will use some of the results of the authors of Ref. [10].

[3] In relativistic units ($\hbar = c = 1$, where $\hbar = h/2\pi$ is the Plank reduced constant and c is the speed of light) $\tau_i = l_i, i = c, h$ because partons and hadrons move with near light speeds.

and τ_h (l_h) is the yo-yo formation time (length). The yo-yo formation means that the colorless system with the valence contents and quantum numbers of the final hadron is formed, but without its "sea" partons. In the two-dimensional string model, which satisfies the conditions where (i) quark-antiquark pairs arising from the vacuum do not have energy and (ii) the energy loss of the leading quark on unit length (string tension) is constant (a widely known example is the Lund model), there is a simple connection between τ_h and τ_c

$$\tau_h - \tau_c = z\nu/\kappa, \tag{9}$$

where κ is the string tension. The average value of τ_c in the standard Lund model has the form

$$\tau_c = \int_0^\infty l dl\, D_c(L, z, l) \Big/ \int_0^\infty dl\, D_c(L, z, l). \tag{10}$$

Following Refs. [18,20], we will use two expressions for the calculation of τ_c. The first one is obtained for the hadrons containing the leading quark (see, for instance, Ref. [9]). This means that the second term within the large brackets in Eq. (4) is omitted and we obtain a very simple expression

$$\tau_c = (1 - z)\nu/\kappa. \tag{11}$$

The meaning of this expression is the following. The color string fully spends its energy at the distance of $L = \nu/\kappa$ beginning from the DIS point. The last hadron produced from the string contains a leading quark and carries an energy E_h. At the distance L, the energy of the leading quark becomes equal to zero and the entire energy of the hadron is concentrated in another constituent. This constituent collects its energy from the string and will have energy E_h on distance L only if it was produced on distance $E_h/\kappa = z\nu/\kappa$ before L. This is reflected in Eq. (11). It is important to note that the hadron produced on the fast end of the string is not always necessarily the fastest hadron. The second expression corresponds to the average value of τ_c in the standard Lund model [Eq. (10)] without any additional suppositions.

Unfortunately, it is impossible to obtain σ^{str} from perturbative QCD, at least in the region $\Delta x \sim \tau$. This means that some model for the shrinkage-expansion mechanism has to be introduced. In this work we use two versions of σ^{str}, which correspond to the smallest χ^2 from Tables I and II of Ref. [20]. The first of them has the quadratic dependence of the cross section on the variable $\Delta x/\tau$. Let us briefly discuss the physical reason behind quadratic dependence. In the naive parton model the inelastic cross section of a hadron with a nucleon is proportional to the transverse area, which is filled in by its partons [i.e., σ^{str} increases proportionally to $(\Delta x/\tau)^2$, where $\tau = \tau_c + c\Delta\tau$, $\Delta\tau = \tau_h - \tau_c$). The parameter c ($0 < c < 1$) is one of the important parameters of improved two-scale model (ITSM) [18]. It was introduced in the model to take into account the well-known fact that the string starts to interact with the hadronic cross section soon after the creation of the first constituent quark of the final hadron and before the creation of the second constituent.

The version following from the naive parton model has the form

$$\sigma^{str}(\Delta x, \tau_c) = \theta(\tau - \Delta x)[\sigma_q + (\sigma_h - \sigma_q)(\Delta x/\tau)^2] + \theta(\Delta x - \tau)\sigma_h. \tag{12}$$

The second version has an exponential form and quadratic dependence from the variable

$$\sigma^{str}(\Delta x, \tau_c) = \sigma_h - (\sigma_h - \sigma_q)\exp\left[-\left(\frac{\Delta x}{\tau}\right)^2\right]. \tag{13}$$

It is worth noting that at small values of Δx these cross sections coincide. The functions τ_c and σ^{str} are important ingredients of ITSM. To date, the choice of these functions is not unique. In our previous studies [18,20] we looked at several options and the best functions were determined by the fit. In this paper we use the combinations of the functions and parameters that correspond to the smallest values of $\hat{\chi}^2$ from Ref. [20] ($\hat{\chi}^2$ denotes the reduced χ^2, which is defined as $\hat{\chi}^2 = \chi^2/\text{d.o.f.}$, where d.o.f. denotes "degree of freedom"). The interested reader can find all the variants of the used functions, the corresponding values of $\hat{\chi}^2$, and the values of the parameters obtained as a result of the fit to the data in our previous work [20].

III. RESULTS AND DISCUSSION

As we already mentioned, we use here the functions and the parameters obtained as a result of the fit to the HERMES data in our previous paper [20]. They are two sets of functions and parameters corresponding to the minimal values of $\hat{\chi}^2$ in Tables I and II from Ref. [20].

In the following we will denote them as set 1 and set 2. The expressions for τ_c and σ^{str} were presented in the previous section, other functions and parameters that are used in this paper will be discussed below. In the range of low energies the formation lengths of the hadrons are short enough, therefore the interactions of the produced hadrons in the final state are very important. Unfortunately, at low energies the information about the sum of the inclusive cross sections for the production of the final pions from all primordial hadrons $\Sigma d\sigma/dz$ is scarce. Undoubtedly, the main term of this sum is the inclusive cross section for the production of the final pion from the initial pion of the same electrical charge. Furthermore, we will use three different reasonable forms for the main term of the sum $d\sigma/dz$ following from the experiment: (i) $d\sigma/dz = \sigma_{in} = 20\,\text{mb}$; (ii) $d\sigma/dz = \sigma/z = 20\,\text{mb}/z$; (iii) $d\sigma/dz$ which was extracted numerically from the experimental data [25,26]. We will express the sum of the cross sections through the main term in the form $\Sigma d\sigma/dz = a \cdot d\sigma/dz$. Taking into account the contributions of other channels we will use for factor a the value larger than unity ($a = 2$ in the calculations).

One of the important parameters of the string model is the string tension (string constant) that determines the energy loss by the leading quark on unit length. In calculations it was fixed at a static value determined by the slope α'_R of the Regge trajectory

$$\kappa = 1/(2\pi\alpha'_R) = 1\,\text{GeV/fm}. \tag{14}$$

The following nuclear density functions (NDF) were used for the calculations. (i) For deuterium the hard-core deuteron wave functions were used. (ii) For light nuclei the shell model wave

functions were used

$$\rho(r) = \rho_0 \left(\frac{4}{A} + \frac{2}{3} \frac{(A-4)}{A} \frac{r^2}{r_A^2} \right) \exp\left(-\frac{r^2}{r_A^2} \right), \qquad (15)$$

where $r_A = 2.47$ fm for ^{12}C. (iii) For the middle and heavy nuclei (^{27}Al, ^{56}Fe, and ^{207}Pb) the Woods-Saxon distribution was used

$$\rho(r) = \rho_0 / \{1 + \exp[(r - r_A)/a)]\}, \qquad (16)$$

where the parameter a is approximately the same for all the nuclei $a \approx 0.54$ fm and parameter r_A is taken in the form $r_A = \left(1.19A^{1/3} - \frac{1.61}{A^{1/3}}\right)$ fm. The corresponding values of ρ_0 were determined from the normalization condition $\int d^3r\rho(r) = 1$. Let us briefly discuss the choice of the nuclear matter distribution functions. For deuterium the choice of the NDF is not important because the FSI are small. For light nucleus ^{12}C the shell model is used in accordance with our earlier works. Other choices for the ^{12}C density profile can be found, for instance, in Ref. [27]. For the middle and heavy nuclei the preferable NDF is the Woods-Saxon distribution. The values of σ_h (hadron-nucleon inelastic cross section) were set equal to $\sigma_{\pi^+} = \sigma_{\pi^-} = 20$ mb.

In Ref. [20] the fit to the experimental data was performed to tune two parameters: the initial value of the string-nucleon cross section σ_q and coefficient c. Here we use two sets of functions and parameters corresponding to the minimal values of $\hat{\chi}^2$ in Tables I and II of Ref. [20]. In Table I the minimal $\hat{\chi}^2 = 0.50$ was obtained at values of the parameters $\sigma_q = 3.90 \pm 0.10$ mb and $c = 0.161 \pm 0.009$ for the functions τ_c and σ^{str} taken in the form of Eqs. (11) and (12), respectively. In Table II the minimal $\hat{\chi}^2 = 0.67$ was obtained at values of the parameters $\sigma_q = 1.99 \pm 0.14$ mb and $c = 0.068 \pm 0.01$ for functions τ_c and σ^{str} taken in the form of Eqs. (10) and (13), respectively.

In Fig. 1 the ratio R_M^π as a function of the fractional energy z of the positively charged pions is presented. In the calculations were used functions and parameters corresponding to min $\hat{\chi}^2$ in Table I from Ref. [20] (set 1). The experimental data for the three nuclear targets carbon, iron, and lead are represented by circles, squares, and triangles, respectively. The filled (open) symbols denote the measurements performed in the ν range $3.2 < \nu < 3.73$ GeV ($3.73 < \nu < 4.3$ GeV). The solid (dashed) lines are the results of our calculations for the first (second) ν regions. The experimental data are taken from Refs. [22,23]. In Fig. 1(a) we compare the experimental data with the theoretical calculations without FSI contribution. In Figs. 1(b)–1(d) the results of calculations with FSI are represented with the corresponding $d\sigma/dz$ forms presented above in points (i)–(iii), respectively. With the aim of preventing the paper from being overloaded by a large number of experimental data, we chose for presentation only the middle bin of Q^2 (i.e., $1.33 < Q^2 < 1.76\,\mathrm{GeV}^2$ from Ref. [22]). The error bars are statistical only. It is easy to see that the theory without FSI [Fig. –1(a)] underestimates the data. Calculations with FSI [Figs. 1(b)–1(d)] describe the experimental data better. In particular, $d\sigma/dz$ taken in form (iii) [Fig. 1(d)] allows to quantitatively describe the entire region of z.

In Fig. 2 the ratio R_M^π as a function of the energy of the virtual photon ν is presented. As in the previous case, data for

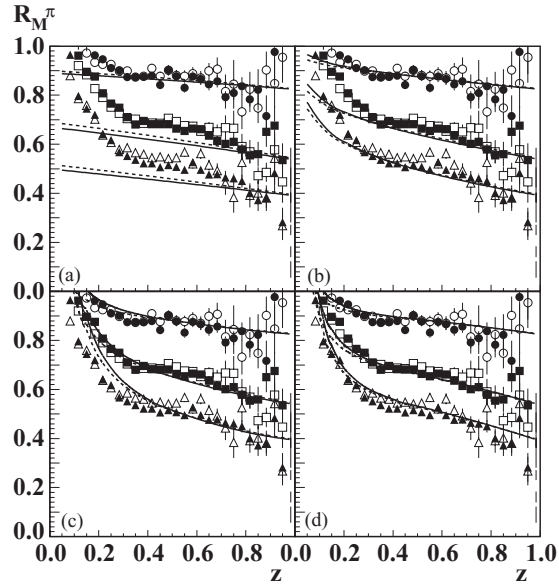

FIG. 1. Ratio R_M^π as a function of the fractional energy z of the positively charged pions. The data for the three nuclear targets carbon, iron, and lead are represented by circles, squares, and triangles, respectively. Filled (open) symbols denote measurements performed in the ν range $3.2 < \nu < 3.73$ GeV ($3.73 < \nu < 4.3$ GeV). Solid (dashed) lines are results of our calculations for the first (second) ν range. Experimental data are taken from Refs. [22,23]. The error bars are statistical only. The functions and parameters from set 1 are used in the calculations. For details see the text.

positively charged pions are presented. The results for the three nuclear targets carbon, iron, and lead are represented by circles, squares, and triangles, respectively. The filled (open) symbols denote the measurements performed in the z region $0.4 < z < 0.5$ ($0.5 < z < 0.6$). The solid (dashed) lines are the results of our calculations for the first (second) z region. As in the previous case, only data from the middle Q^2 bin are included. The experimental data are taken from Refs. [22,23]. The error bars are only statistical. As in the case of z dependence [Fig. 1] the theory without FSI [Fig. 2(a)] underestimates the data. The calculations with FSI [Figs. 2(b)–2(d)] describe the experimental data better.

In Fig. 3 the ratio R_M^π as a function of the fractional energy z of the positively charged pions is presented. In calculations were used the functions and parameters corresponding to min $\hat{\chi}^2$ in Table II from Ref. [20] (set 2). The experimental data are the same as in Fig. 1. In Fig. 3(a) we compare the experimental data with the theoretical calculations without FSI. In Figs. 3(b)–3(d) the results of the calculations with FSI are presented that correspond to $d\sigma/dz$ with the forms presented above in points (i)–(iii), respectively. It is easy to see that the theory without FSI [Fig. 3(a)] underestimates the data. The calculations with FSI [Figs. 3(b)–3(d)] describe the experimental data better.

In Fig. 4 the ratio R_M^π as a function of the energy of the virtual photon ν is presented. In the calculations were used functions and parameters corresponding to min$\hat{\chi}^2$ in Table II from Ref. [20] (set 2). The experimental data are the same as in Fig. 2. As in the case of z dependence

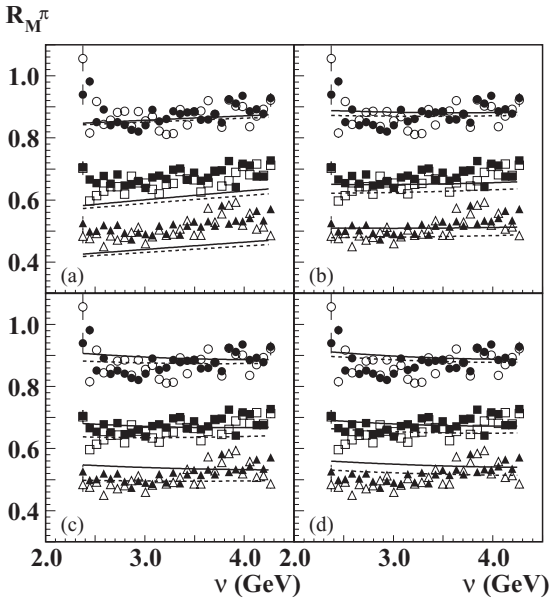

FIG. 2. Ratio R_M^π as a function of the energy of the virtual photon ν. The data for the three nuclear targets carbon, iron, and lead are represented by circles, squares, and triangles, respectively. Filled (open) symbols denote measurements performed in the z range $0.4 < z < 0.5$ ($0.5 < z < 0.6$). Solid (dashed) lines are results of our calculations for the first (second) z range. Experimental data are taken from Refs. [22,23]. The error bars are statistical only. The functions and parameters from set 1 are used in the calculations. For details see the text.

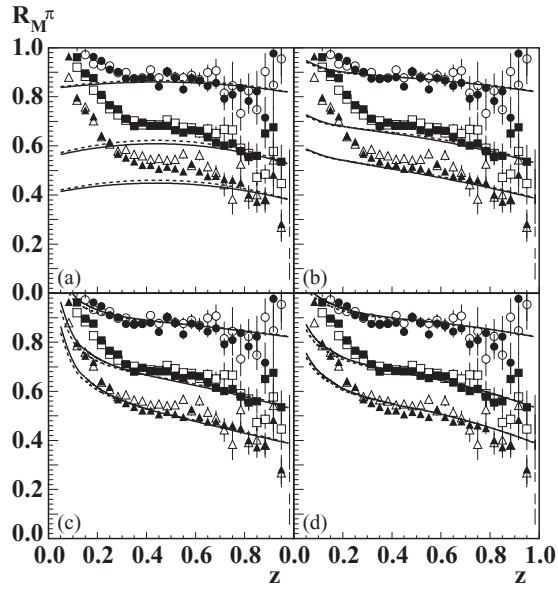

FIG. 3. Ratio R_M^π as a function of the fractional energy z of the positively charged pions. The data for the three nuclear targets carbon, iron, and lead are represented by circles, squares, and triangles, respectively. Filled (open) symbols denote measurements performed in the ν region $3.2 < \nu < 3.73$ GeV ($3.73 < \nu < 4.3$ GeV). Solid (dashed) lines are the results of our calculations for the first (second) ν region. Experimental data are taken from Refs. [22,23]. The error bars are statistical only. The functions and parameters from set 2 are used in the calculations. For details see the text.

[Fig. 3] the theory without FSI [Fig. 4(a)] underestimates the data. The calculations with FSI [Figs. 4(b)–4(d)] describe the experimental data better. The comparison of the results of Figs. 1–4 seems to indicate that set 1 is preferred by the data. The reason for this is the definition of l_c. In set 1 l_c is used for hadrons containing the leading quark, which is the model-free quantity, while in set 2 the average value of l_c, $\langle l_c \rangle$ is used, which is obtained in the framework of the Lund standard model. $\langle l_c \rangle$ is obtained under the assumption that the multiplicity of the final hadrons changes from 2 to infinity, which is a rough approximation for the case of low energies.

In Fig. 5 the aluminum-deuteron ratio R_M^π as a function of the fractional energy z of the positively (filled circles) and negatively (filled squares) charged pions is presented at the fixed virtual photon's energy $\nu = 3.794$ GeV. The experimental data are taken from Ref. [24]. The error bars are only statistical.

Let us discuss in detail the theoretical lines in this figure. (i) The solid line is the result of calculations in the framework of our model (ITSM) with the functions and parameters presented above. Note that in these calculations we used the following values for σ_h (hadron-nucleon inelastic cross section): $\sigma_{\pi^+} = \sigma_{\pi^-} = 20$ mb. (ii) The dashed line is also the result of calculations in the framework of our model (ITSM), but with the other value of the hadron-nucleon inelastic cross section: $\sigma_{\pi^+} = \sigma_{\pi^-} = 25$ mb. Two other cases, (iii) the dotted line and (iv) dot-dashed line, are the results of theoretical calculations in the "Glauber's limit," which corresponds to

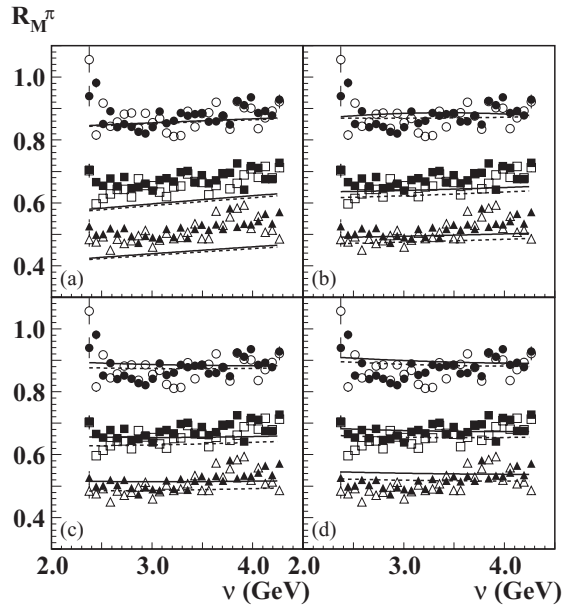

FIG. 4. Ratio R_M^π as a function of the energy of the virtual photon ν. The data for the three nuclear targets carbon, iron, and lead are represented by circles, squares, and triangles, respectively. Filled (open) symbols denote measurements performed in the z region $0.4 < z < 0.5$ ($0.5 < z < 0.6$). Solid (dashed) lines are the results of our calculations for the first (second) z region. Experimental data are taken from Refs. [22,23]. The error bars are statistical only. The functions and parameters from set 2 are used in the calculations. For details see the text.

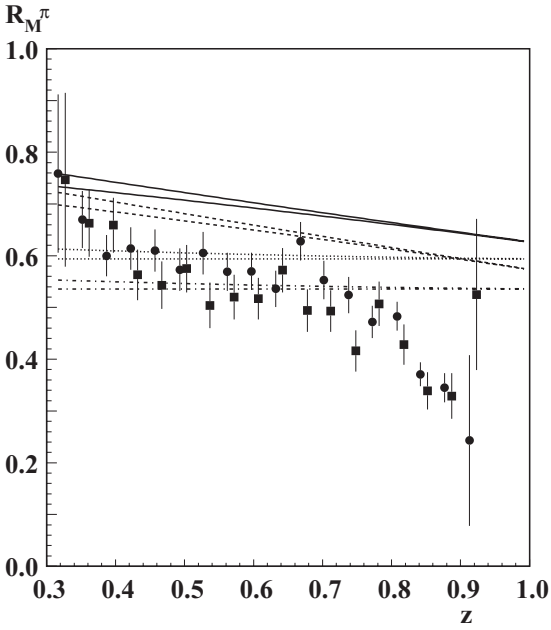

FIG. 5. The aluminum-deuteron ratio R_M^π as a function of the fractional energy z of the positively (filled circles) and negatively (filled squares) charged pions is presented at a fixed virtual photon's energy $\nu = 3.794$ GeV. Experimental data are taken from Ref. [24]. The error bars are statistical only. The functions and parameters from set 1 are used in the calculations. Details of theoretical calculations are given in the text.

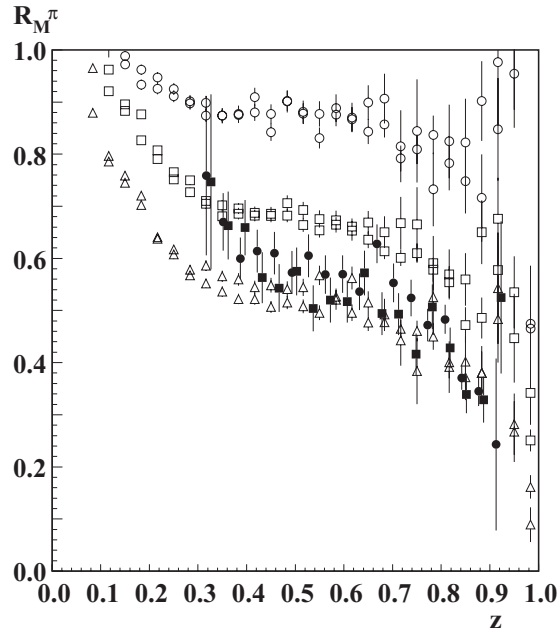

FIG. 6. Ratio R_M^π as a function of the fractional energy of pions z. The results of two experiments are compared. Open symbols represent the first set of data [22,23] for positively charged pions in two bins of ν in the case of three nuclear targets (circles represent carbon, squares are iron, and triangles are lead), filled symbols represent the second set of data [24] for positively (filled circles) and negatively (filled squares) charged pions in the case of the aluminum target.

the supposition that, beginning from the DIS point string, prehadrons and hadrons are absorbed in the nuclear medium with the hadronic cross sections equal in the case (iii) $\sigma_{\pi^+} = \sigma_{\pi^-} = 20$ mb and in the case (iv) $\sigma_{\pi^+} = \sigma_{\pi^-} = 25$ mb.

We use two values of the pion-nucleon inelastic cross section σ_π for the calculations because in the energy range of pions from 1 to 4 GeV, as in this experiment, σ_π for positively and negatively charged pions varies between 20–25 mb (it is more accurate to say that σ_{π^+} is close to 21 mb, σ_{π^-} is close to 25 mb).

In the calculations were used functions and parameters corresponding to minimal $\hat{\chi}^2$ in Table I from Ref. [20] (set 1). The bottom lines of each kind correspond to calculations without FSI, the top lines correspond to calculations with FSI [where $d\sigma/dz$ is taken in form (i)]. We see that the case of aluminum target corrections due to FSI are small and cannot improve the description of the data. Calculations performed with other versions of $d\sigma/dz$, as well as calculations performed with the functions and parameters from set 2, give close results and therefore are not presented.

In models in which the absorption of the particles in a nuclear environment is considered as a cause of NA, "Glauber's limit" is not reachable because the absorption cross sections of prehadrons are much smaller than the absorption cross sections of the real hadrons. A comparison of the theoretical calculations with the experimental data gives an unexpected result, which consists of the fact that the data agree with the "Glauber's limit" on value, but have the pronounced slop. If this result is related to the kinematics of JLab, in particular to the energy range of JLab, then it should be common to both sets of data. Therefore it is interesting to compare the two sets of data obtained at JLab, which we will do in the next figure.

In Fig. 6 the ratio R_M^π as a function of the fractional energy z of pions is presented. The results of two experiments are compared. The open symbols represent the first set of data [22,23] for positively charged pions in both bins of ν in the case of the three nuclear targets (the circles represent carbon, squares are iron, and triangles are lead), the filled symbols represent the second set of data [24] for positively (filled circles) and negatively (filled squares) charged pions on an aluminum target. It is easy to see that the multiplicity ratio for ^{27}Al from the second set of data settles down between the multiplicity ratios of the heavier nuclei ^{56}Fe and ^{207}Pb from the first set of data. One might even say that the data for ^{27}Al are closer to the data for ^{207}Pb than to the data for ^{56}Fe. For the quantitative comparison of the two sets of data we performed a fit to the data in the region $0.3 \leqslant z \leqslant 0.95$ using the functions and parameters from Table I of Ref. [20]. FSI were calculated with $d\sigma/dz$ in form (iii). As a result, for data from the authors of Refs. [22,23] we obtained $\hat{\chi}^2 = 2.27$ while for the data from Ref. [24] we obtained $\hat{\chi}^2 = 26.8$. In our opinion it means that there is a definite discrepancy between the two sets of data.

IV. CONCLUSION

The NA in SIDIS was studied in the framework of the string model [18,20] for the case where positively and negatively

charged pions were produced on different nuclei at "low energies" ($\nu < 5$ GeV). Two sets of data from Refs. [22–24] from JLab were considered. For this case the formalism used for high energies was supplemented by a term that takes into account the FSI (or cascading process). As can be seen from Figs. 1 through 5, this correction is small in size for carbon and aluminum (although in the case of carbon it considerably improves the agreement with the data at low z), however, it is quite a substantial correction for iron and lead.

The string model satisfactorily describes the first set of data except for the region of small z. In the region of small z ($z < 0.3$) there is some discrepancy between the model and experimental data. This is especially evident in Fig. 3 where theoretical curves were obtained with the parameters and functions from Table II of Ref. [20] (set 2). It demonstrates the sensitivity of the model to the parameters and functions and points out the opportunity to extract them better in the future with more precise data. We want to reiterate that the scarcity of data on the inclusive processes has not given us the opportunity to calculate more accurately the contribution of FSI. Another issue that needs to be investigated in this energy region is to find a threshold on z above which the string model works because in this energy region there is no clear separation between the current and target fragmentation regions. The second set of data cannot be described by the string model. In this case the data are closer to Glauber's limit. This is unusual in itself. A definite discrepancy between the two sets of data was found by means of direct comparison.

ACKNOWLEDGMENTS

This work has been partially supported by a cooperation agreement between DESY and YerPhI.

[1] L. S. Osborne *et al.*, Phys. Rev. Lett. **40**, 1624 (1978).
[2] J. Ashman *et al.*, Z. Phys. C **52**, 1 (1991).
[3] M. R. Adams *et al.*, Phys. Rev. D **50**, 1836 (1994).
[4] A. Airapetian *et al.*, Eur. Phys. J. C **20**, 479 (2001).
[5] A. Airapetian *et al.*, Phys. Lett. B **577**, 37 (2003).
[6] A. Airapetian *et al.*, Nucl. Phys. B **780**, 1 (2007).
[7] G. Davidenko and N. Nikolaev, Nucl. Phys. B **135**, 333 (1978).
[8] A. Bialas, Acta Phys. Polon. B **11**, 475 (1980); M. Gyulassy and M. Pluemer, Nucl. Phys. B **346**, 1 (1990).
[9] B. Kopeliovich, Phys. Lett. B **243**, 141 (1990).
[10] J. Czyzewski and P. Sawicki, Z. Phys. C **56**, 493 (1992).
[11] R. G. Badalyan, Z. Phys. C **55**, 647 (1992).
[12] A. Accardi, V. Muccifora, and H. J. Pirner, Nucl. Phys. A **720**, 131 (2003); A. Accardi, D. Gruenewald, V. Muccifora, and H. J. Pirner, *ibid.* **761**, 67 (2005).
[13] F. Arleo, Eur. Phys. J. C **30**, 213 (2003).
[14] T. Falter, W. Cassing, K. Gallmeister, and U. Mosel, Phys. Rev. C **70**, 054609 (2004).
[15] X.-N. Wang and X. Guo, Nucl. Phys. A **696**, 788 (2001); E. Wang and X.-N. Wang, Phys. Rev. Lett. **89**, 162301 (2002).
[16] B. Kopeliovich, J. Nemchik, and E. Predazzi, in *Proceedings of the Workshop on Future Physics at HERA*, edited by G. Ingelman, A. De Roeck, and R. Klanner (DESY, Hamburg, Germany, 1996), Vol. 2, p. 1038; B. Kopeliovich *et al.*, Nucl. Phys. A **740**, 211 (2004).
[17] N. Akopov, G. Elbakian, and L. Grigoryan, arXiv:hep-ph/0205123.
[18] N. Akopov, L. Grigoryan, and Z. Akopov, Eur. Phys. J. C **44**, 219 (2005).
[19] N. Akopov, L. Grigoryan, and Z. Akopov, Eur. Phys. J. C **52**, 893 (2007).
[20] N. Akopov, L. Grigoryan, and Z. Akopov, Eur. Phys. J. C **70**, 5 (2010).
[21] R. Sassot, M. Stratmann, and P. Zurita, Phys. Rev. D **81**, 054001 (2010).
[22] H. Hakobyan (CLAS Collaboration), Ph.D. thesis, Yerevan State University, Armenia, 2008.
[23] W. Brooks and H. Hakobyan, Nucl. Phys. A **830**, 361C (2009); AIP Conf. Proc. **1056**, 215 (2008).
[24] R. Asaturyan *et al.*, arXiv:1103.1649.
[25] D. Crennell *et al.*, Phys. Rev. Lett. **28**, 643 (1972).
[26] M. Alston-Garnjost *et al.*, Phys. Lett. B **39**, 402 (1972).
[27] H. de Vries, C. W. de Jager, and C. de Vries, Atom. Data Nucl. Data Tables **36**, 495 (1987).